IEEE Access
Multidisciplinary | Rapid Review | Open Access Journal

Received 11 July 2022, accepted 28 August 2022, date of publication 5 September 2022, date of current version 4 October 2022.

Digital Object Identifier 10.1109/ACCESS.2022.3204400

RESEARCH ARTICLE

A Wide-Angle and High-Efficiency Reconfigurable Reflectarray Antenna Based on a Miniaturized Radiating Element

SUN-GYU LEE[1], YONG-HYUN NAM[1], YONGJUNE KIM[2], (Member, IEEE), JONGYEONG KIM[3], AND JEONG-HAE LEE[1], (Senior Member, IEEE)

[1]Department of Electronic and Electrical Engineering, Hongik University, Seoul 04066, Republic of Korea
[2]Department of Electrical Engineering, The University of Suwon, Hwaseong, Gyeonggi-do 18323, Republic of Korea
[3]Specific Radar Team, Hanwha Systems, Yongin, Gyeonggi-do 17121, Republic of Korea

Corresponding author: Jeong-Hae Lee (jeonglee@hongik.ac.kr)

This research has been supported by a grant-in-aid of HANWHA SYSTEMS based on the Defense Challengeable Future Technology Program of the Agency for Defense Development (ADD).

ABSTRACT A wide-angle reconfigurable reflectarray antenna (RRA) utilizing a miniaturized ring patch that can be efficiently controllable with a single bit is designed and experimentally verified. Based on the adoption of miniaturized radiating element and the elaborate study to optimize quantization efficiency considering reference phase and asymmetric phase difference, highly directive beam scanning is achieved in a wide $\pm 60°$ range in both the H- and E- planes. Furthermore, the feeding structure to minimize focal diameter ratio (F/D) and maximize feeding efficiency such as illumination and spillover Efficiencies is studied, resulting in a low profile configuration with F/D=0.36. The fabricated RRA prototype was measured at 9.85 GHz (X-band) with the highest aperture efficiency of 28% and a 1 dB gain bandwidth of 530 MHz, respectively.

INDEX TERMS Metasurface, PIN diode, 1-bit, asymmetric phase difference, phase quantization.

I. INTRODUCTION

Reconfigurable reflectarray antennas (RRAs) [1], [2], [3] are hybrid-type antennas that combine a high-gain parabolic and electronically beam-steerable phased array antenna. Based on a low insertion loss and simplified strategy for phase modulation, RRAs have enormous merits from the perspectives of aperture efficiency and other factors, such as cost, size, and weight. Therefore, RRAs have attracted great attention as promising alternatives for the conventional systems used in satellite communications and radars.

To control the phase of the reflection coefficient of each RRA unit cell, electronically tunable components, such as a PIN diode [4], [5], [6], [7], varactor diodes [8], liquid crystal [9], or Radio-frequency micro-electro-mechanical system (RF-MEMS) switch [10], have been utilized. In particular, PIN diode-based RRAs require discrete voltage controls that enable simplified antenna systems. In addition, they are suitable for high-speed beam scanning based on the fast on/off switching speed of the PIN diode.

Despite the merits of the RRAs based on the PIN diode, early RRAs in [11], [12] had limited beam scanning range and relatively low aperture efficiency. To address these limitations, subsequent studies have been conducted to optimize the aperture efficiency composed of spillover, illumination, element-reflection, and phase-quantization efficiencies [5], [6], [7], [13]. However, the previous RRAs in [5], [6], [7] had relatively bulky feeding structures, where the focal diameter ratio (F/D) is close to 1. Note that the focal length and the size of the aperture are indicated by F and D. Moreover, the relatively large unit cells of an RRA are thought to limit beam-scanning ranges [5], [7].

A high aperture efficiency, wide-angle scanning, and low profile configurations are advantageous for practical applications. To enhance aperture efficiency, a technique that optimizes the relative phase distribution of the metasurface by

The associate editor coordinating the review of this manuscript and approving it for publication was Tutku Karacolak.

adjusting the reference phase has been presented [5], [6], [7], [14]. It can mitigate the degradation of the aperture efficiency, which is partially related to the quantization of the phase distribution using the unit cell that has a 180° phase difference between the on/off states of a PIN diode. In addition, another technique that optimizes the focal length of the feeding structure to enhance aperture efficiency while designing with a low profile has been studied [14]. Meanwhile, to extend the beam scanning range of the array antenna, a miniaturized radiating element that guarantees a wide element beam pattern has been proposed [15].

In this study, a wide-angle beam steerable RRA is proposed and experimentally verified in the X-band using an efficient 1-bit control. By adopting the miniaturized unit cell for the wide element pattern [15], wide beam-scanning ranges are achieved in both the H- and E- planes while maintaining high aperture efficiencies. In addition, a low-gain feed horn is adopted, and its position is carefully optimized for a low profile and high illumination and spillover efficiencies [14]. In particular, it was found that the phase difference between the on and off states is not necessarily 180° for the maximum aperture efficiency. A well-integrated prototype of the designed RRA of the 12 × 12 metasurface was fabricated and experimentally verified.

II. DESIGN

A. MINIATURIZED UNIT CELL

The miniaturized unit cell is designed based on the copper-ring patch, and its geometry is shown in Fig. 1(a) and (b). The unit cell consists of two dielectric substrates of Taconic TLY-5 ($\varepsilon_r = 2.2$, $\tan\delta = 0.0009$), where the thicknesses of the upper and lower substrates are 1.575 and 0.508 mm, respectively. The radiating ring patch with the PIN diode is located on the upper substrate and is connected to the ground through a shorting via hole with a diameter of 0.4 mm. A bias line to induce a driving voltage and a radial stub to isolate a RF current are added to the bottom of the lower substrate.

Because the sizes of conventional rectangular or square patches is reduced using the ring patch by increasing the series inductance and by locating the PIN diode inside the ring, this miniaturized ring patch broadened the radiation pattern to guarantee wide-angle beam scanning [15]. From the perspective of miniaturization, it is well known that the periodicity of the element smaller than quarter wavelength deteriorates the performance of beam steering owing to tight mutual couplings among the unit cells [3]. On the other hand, the element periodicity greater than half wavelength may cause a grating lobe in the radiating region [3]. To prevent the mutual couplings and the grating lobe, the period of the unit cell P and the length of the ring patch L were properly chosen to be 10.5 mm (=$\lambda_0/3$) and 6.11 mm (=$\lambda_0/5$), respectively. It is also mentioned that the other geometric parameters are $W = 0.75$ mm, sL=1 mm, and the gap between ring patch and shorting via patch is 0.2 mm.

The unit cell reradiates an incident electromagnetic (EM) wave by operating as a half wavelength resonator for the off

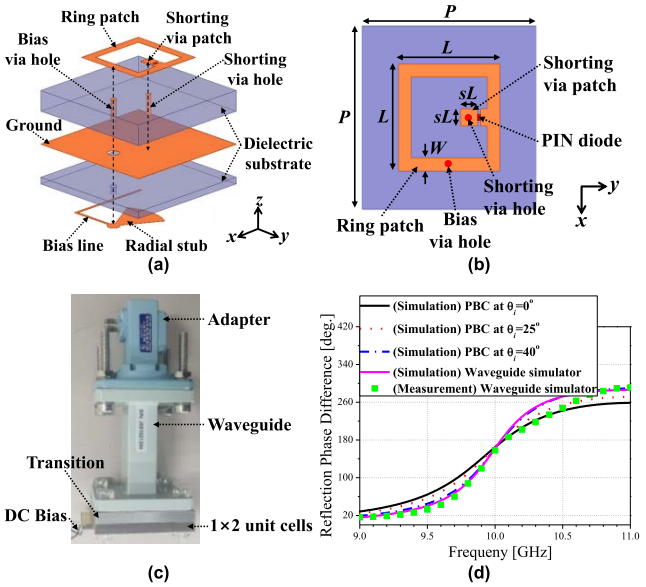

FIGURE 1. Miniaturized unit cell, (a) 3-D schematic and (b) top view of it, (c) setup of waveguide simulator, and (d) reflection-phase difference between on and off states of PIN diode.

state of the PIN diode at 10.1 GHz. When the PIN diode is turned on, the ring patch is electronically connected to the ground, and it supports 3/4 wavelength resonant modes, of which the resonance frequency is shifted upward compared to that of the off state [5], [6], [7]. For operation at the X band, a MA4GP907 PIN diode of MACOM was adopted. When the PIN diode is turn on, it can be modeled as a series circuit composed of a resistor and an inductor, of which the resistance and inductance are 4.2 Ω and 0.05 nH, respectively. On the other hand, when the PIN diode is turn off, it can be modeled as a parallel circuit of a resistor and capacitor, of which the resistance and capacitance are 300 kΩ and 50 fF, respectively.

The unit cell designed with the periodic boundary condition (PBC) was simulated and measured using a WR-90 waveguide to verify its phase responses [7]. Here, the simulation and measurement were performed using the ANSYS HFSS full-wave simulator using the setup in Fig. 1(c). To match the size of the sample composed of 1 × 2 unit cells (21 × 10.5 mm^2) and the aperture area of the waveguide (22.86 × 10.16 mm^2), an aluminum transition was inserted between the waveguide and sample, which tapered the area of the waveguide to that of the sample. Fig. 1(d) shows a simulation and measurement of reflection-phase difference as the state of the PIN diode is turned on or off. The 180° phase difference was confirmed around 10.1 GHz, regardless of the incident angle. Since the TE_{10} mode propagates in the waveguide, the incident angle of TE_{10} mode is 40°. For this reason, the waveguide simulator well matches the PBC with an incident angle of 40°. When considering the small incident angle, i.e., 0° or 25°, the phase difference curves at small incident angle are a slight difference from that at incident angle of 40°.

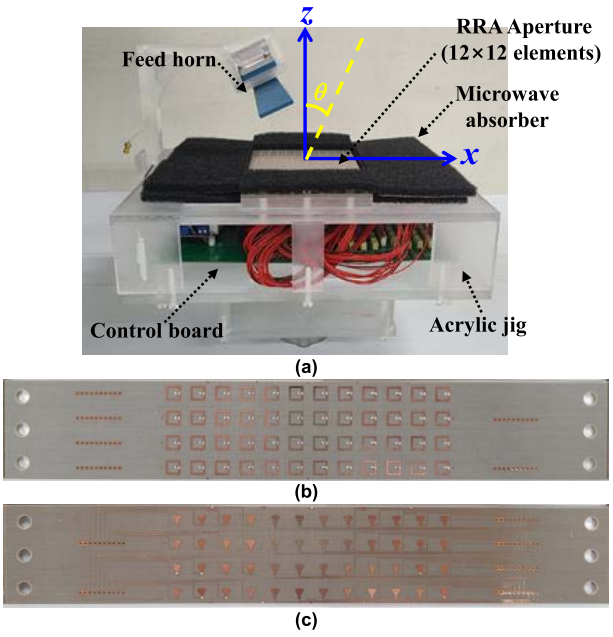

FIGURE 2. Fabricated structure of RRA. (a) RRA prototype, (b) top, and (c) bottom views of 4 × 12 RRA module.

B. RECONFIGURABLE REFLECTARRAY ANTENNA

A well-integrated RRA prototype that is composed of 12 × 12 miniaturized 1-bit unit cells was designed as shown in Fig. 2(a). The RRA aperture was attached to an acrylic jig that supports a feed horn above the RRA and a control board under the ground. Microwave absorbers were attached around the RRA to minimize undesired reflections from the acrylic jig. Fig. 2(b) and (c) show the top and bottom views of a 4 × 12 RRA module that is a part of the 12 × 12 RRA prepared to guarantee the replacement of damaged unit cells. The bias lines in Fig. 2(c) are connected to the control board through pitch connectors and harness cables.

To maximize aperture efficiency while designing with the low profile RRA, an analysis of the maximum feeding efficiency and F/D according to the gain of feed antenna [14] is performed. The feeding efficiency is defined as the product of illumination and spillover efficiencies. According to previous study in [14], a high gain feed antenna provides high feeding efficiency, but requires a bulky feed structure i.e., F/D is close to 1. On the other hand, if a low gain feed antenna is adopted and its position is carefully optimized, the RRA can be designed with a low profile at the cost of slightly reduced feeding efficiency.

Comparing several commercial horns by observing the feeding efficiency in HFSS simulations, it was confirmed that a 11 dBi horn has slightly low feeding efficiency (∼1%) but the F/D reduced by about half (=57%) compared to a 15 dBi horn. Therefore, the low-gain 11 dBi horn antenna was finally selected. The polarization of the feed horn was set to horizontal polarization (E_y) to match it with the polarization of the unit cell. An offset angle of the feed horn was set to −25° in the *xoz* plane through a parametric study in the HFSS simulation to avoid a feed blockage. As a result, the feed horn was located at (−30, 0, 63) mm, and the F/D was calculated as 0.36. The illumination and spillover efficiencies were 82.1% and 83.5%, respectively. The feeding efficiency was calculated as 68.6%.

C. BEAM CONTROL WITH 1-BIT QUANTIZATION

By manipulating the wavefront of the reflected wave from the RRA aperture, beam steering in an arbitrary direction is achieved. The phase of the reflected wave from each unit cell, or the output phase $\varphi_{(m,n)}^{\text{output}}$, can be presented using the following array factor [16]:

$$\varphi_{(m,n)}^{\text{output}} = \left(-\frac{M-1}{2}+m-1\right)\beta_x + \left(-\frac{N-1}{2}+n-1\right)\beta_y \tag{1}$$

where $\beta_x = -kd_x \sin\theta\cos\phi$ and $\beta_y = -kd_y \sin\theta\sin\phi$ are progressive phase shifts in the x- and y-directions, respectively. M and N are the number of elements on the RRA aperture in the x- and y-axes, respectively. Also, m and n are orders that indicate the locations of the unit cell in the x- and y-axes, respectively.

The output phase $\varphi_{(m,n)}^{\text{output}}$ can be analyzed from the phase of the incident EM wave from the feed horn and that of the reflection coefficient of the unit cell:

$$\left\{\varphi_{(m,n)}^{\text{output}} + \Delta\varphi\right\} = \varphi_{(m,n)}^{\text{input}} + \left\{\varphi_{(m,n)}^{\text{required}} + \Delta\varphi\right\}, \tag{2}$$

where the input phase $\varphi_{(m,n)}^{\text{input}}$ and the required phase $\varphi_{(m,n)}^{\text{required}}$ indicate the phase of the illuminated EM wave of the unit cell of (m, n)-th and that of the reflection coefficient of the unit cell located at (m, n), respectively. The input phase of E_y is calculated using the field calculator in HFSS simulator. The required phase can be calculated in a way that shifts the input phase to that of the EM wave reflected in a targeted direction. The shift of the reference phase $\Delta\varphi$ can be added equally across all unit cells, but it does not affect the beam performance in case of continuous phase control.

If 1-bit phase control is considered, the term of $\varphi_{(m,n)}^{\text{required}} + \Delta\varphi$ can be quantized into two states of 0 and $\Delta\varphi_{1\text{-bit}}$:

$$-180^\circ + \Delta\varphi_{1\text{-bit}}/2 \le \varphi_{(m,n)}^{\text{required}} + \Delta\varphi < \Delta\varphi_{1\text{-bit}}/2$$
$$\rightarrow \varphi_{(m,n)}^{\text{required}} + \Delta\varphi \cong \varphi_{(m,n)}^{\text{required, 1-bit}} = 0^\circ \tag{3-1}$$
$$\Delta\varphi_{1\text{-bit}}/2 \le \varphi_{(m,n)}^{\text{required}} + \Delta\varphi < 180^\circ + \Delta\varphi_{1\text{-bit}}/2$$
$$\rightarrow \varphi_{(m,n)}^{\text{required}} + \Delta\varphi \cong \varphi_{(m,n)}^{\text{required, 1-bit}} = \Delta\varphi_{1\text{-bit}}, \tag{3-2}$$

where the 1-bit quantized required phase $\varphi_{(m,n)}^{\text{required, 1-bit}}$ indicates a quantized value of $\varphi_{(m,n)}^{\text{required}} + \Delta\varphi$. As the required phase is quantized, the aperture efficiency decreases owing to the quantization error. By properly choosing the appropriate $\Delta\varphi$ and $\Delta\varphi_{1\text{-bit}}$, quantization error can be minimized. The related results will be discussed in detail in Section IV.

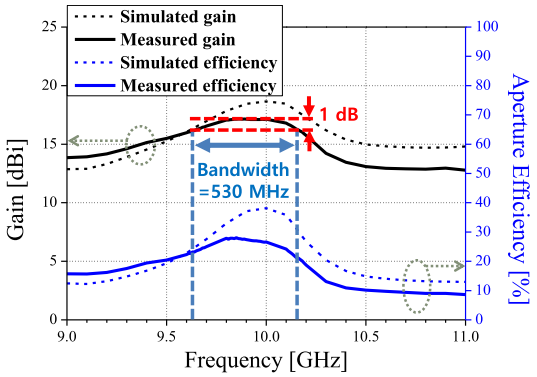

FIGURE 3. Measured 1 dB gain bandwidth for $(\theta, \phi) = (30°, 0°)$.

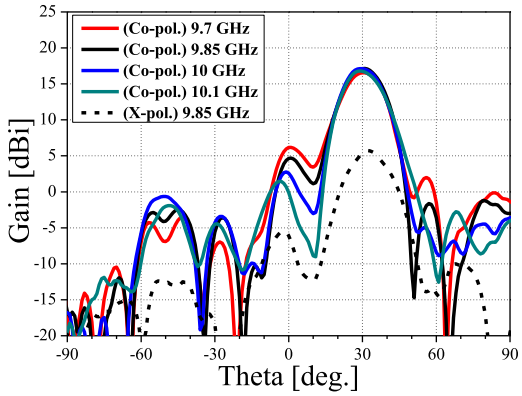

FIGURE 4. Radiation patterns of RRA for $(\theta, \phi) = (30°, 0°)$ at some different frequencies.

III. RESULTS

The fabricated RRA was measured by a Keysight E8362B PNA network analyzer in an anechoic chamber with a distance of 7 m. The aperture efficiency [17] can be calculated using the peak gain as

$$\eta_a = \frac{G(\theta, \phi)|_{\max}}{\frac{4\pi A_{\mathrm{RRA}}}{\lambda^2}\cos\theta}, \tag{4}$$

where A_{RRA} indicates the physical aperture area of RRA, $A_{\mathrm{RRA}} = 126 \times 126\ \mathrm{mm}^2$.

Fig. 3 shows the gain and aperture efficiency as a function of frequency. The beam steering angle was set to $(\theta, \phi) = (30°, 0°)$, which is the direction of the maximum aperture efficiency observed. The measured peak gain and aperture efficiency was confirmed as 17.14 dBi and 28%, respectively, at 9.85 GHz, downshifted from 10.1 GHz for which the unit cell was designed. The measured 1 dB gain bandwidth was also confirmed to be 530 MHz, and the fractional bandwidth is calculated as 5.38%. Fig. 4 indicates the radiation patterns for $(\theta, \phi) = (30°, 0°)$ at some different frequencies. The measured side-lobe level (SLL) and cross-polarization level (CPL) were confirmed as −12.5 dB and −11.4 dB, respectively. The relatively high CPL may be owing to the symmetric feature of the square unit cell.

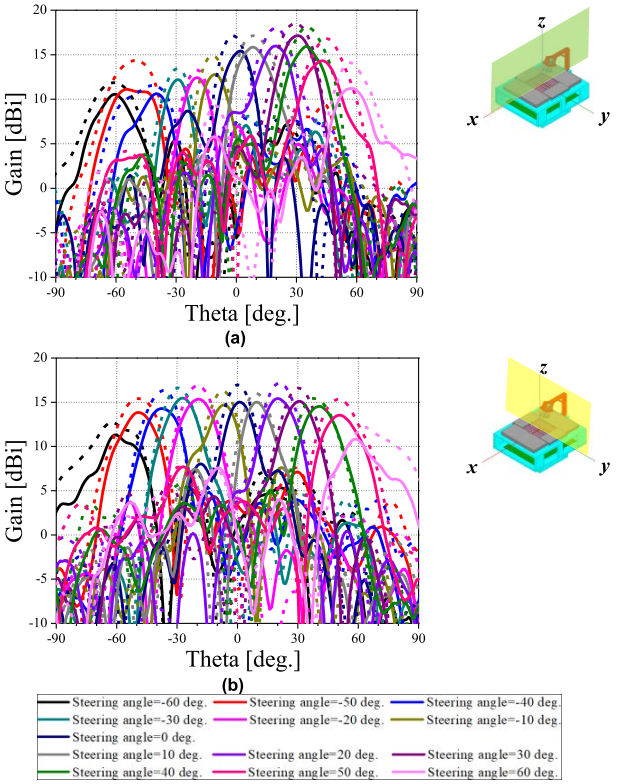

FIGURE 5. Radiation patterns of RRA (a) on the xoz (H-plane) and (b) on the yoz planes (E-plane) at 9.85 GHz. Solid line: measurement, dashed line: simulation.

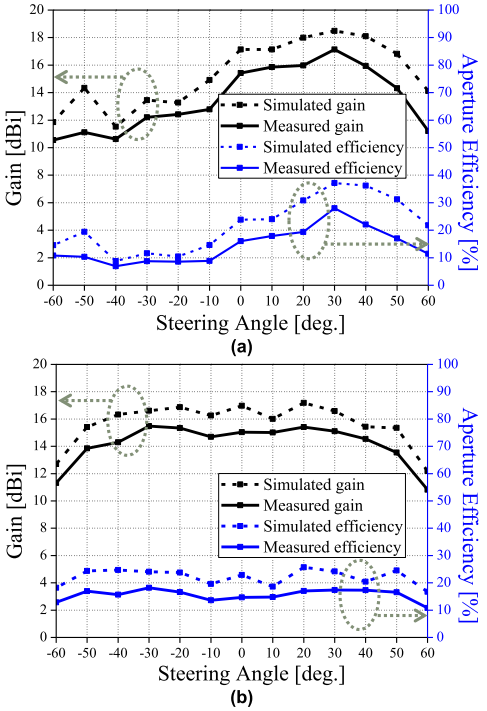

FIGURE 6. Peak gain and aperture efficiency versus beam steering angle (a) on the xoz (H-plane) and (b) on the yoz planes (E-plane) at 9.85 GHz.

The beam scanning performance of the designed RRA was simulated and measured, as shown in Fig. 5(a) and (b),

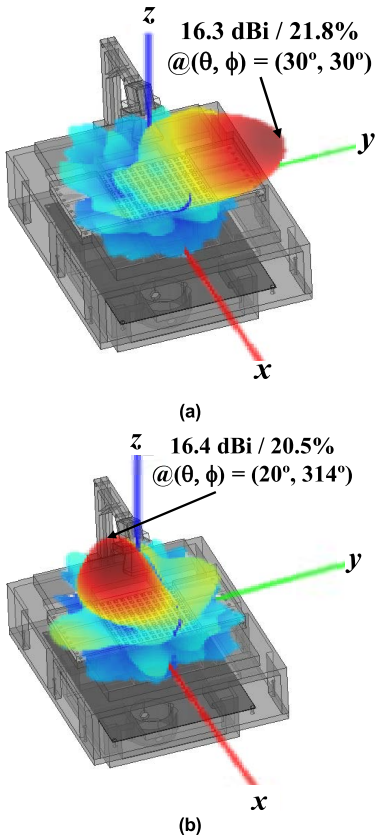

FIGURE 7. Measured 3-D beam pattern for (a) $(\theta, \phi) = (30°, 30°)$ and (b) $(\theta, \phi) = (20°, 315°)$ at 9.85 GHz.

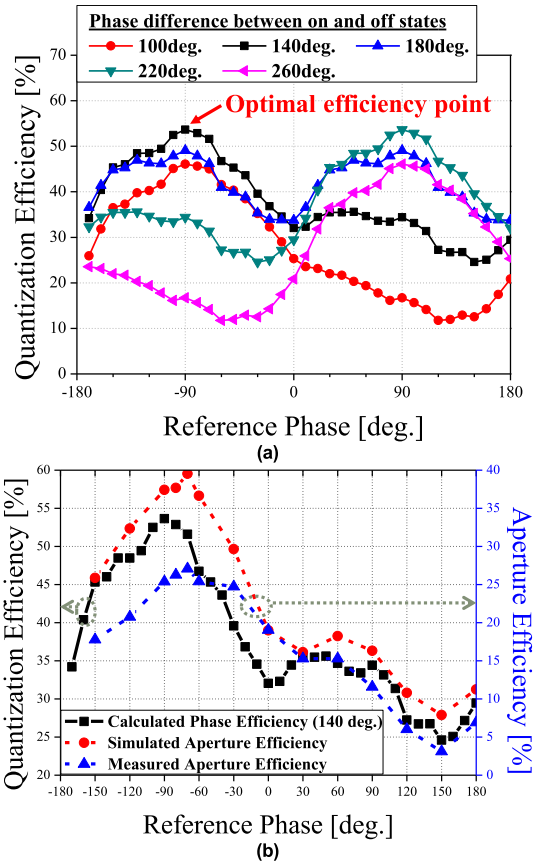

FIGURE 8. Aperture and quantization efficiencies versus reference phases for $(\theta, \phi) = (30°, 0°)$ at 9.85 GHz. (a) Quantization efficiency for various 1-bit phase differences and (b) comparison of calculated, simulated, and measured results at phase difference of 140° between on and off states.

including the results of ±60° beam steering with 10° intervals in the *xoz* and *yoz* planes or *H*- and *E*-planes, respectively. The observation frequency was set to 9.85 GHz, which is the frequency of the maximum aperture efficiency. The simulated and measured peak gains were confirmed as 18 dBi and 17.14 dBi at $(\theta, \phi) = (30°, 0°)$, respectively. The simulated and measured aperture efficiencies were 32.2% and 28%, respectively. Even though the deteriorations by the feed blockage were observed in Fig. 5(a) along the -*x* direction in the *xoz* plane, the beam was well steered up to −60°. The discrepancies between the simulated and measured gains may originate from manufacturing tolerances, a misalignment of the feed horn, and/or an error in modeling the equivalent resistance of the PIN diode. The gain and aperture efficiency for each steering angle are summarized in Fig. 6. To verify the performance of the 3-D beam scanning, the 3-D beam patterns for arbitrary angles $(\theta, \phi) = (30°, 30°)$ and $(\theta, \phi) = (20°, 315°)$ were measured as shown in Fig. 7. A well-defined beam was observed, and the measured gain was confirmed to be 16.3 and 16.4 dBi, respectively.

IV. DISCUSSIONS

As described in Subsection II-*C*, the quantization error can be mitigated by shifting the reference to the required phase. As derived from (3), phase states 0 and $\Delta\varphi_{1\text{-bit}}$ can exist for the 1-bit quantization where the phase difference between two states is indicated by $\Delta\varphi_{1\text{-bit}}$. The quantization efficiency (also referred to as quantization loss in [5], [6]) can be calculated using the following array factor:

$$\eta_q = \frac{\left|\mathrm{AF}\left(\theta,\ \phi\right)_{1\text{-bit}}\right|^2}{\left|\mathrm{AF}\left(\theta,\ \phi\right)_{\text{continuous}}\right|^2}. \tag{5}$$

Fig. 8(a) shows the calculated quantization efficiency vs. the variation in the reference phase for various phase differences between the on and off states, at 40° intervals. In the case of the symmetric phase difference, i.e., $\Delta\varphi_{1\text{-bit}} = 180°$, the same two peaks were found at the reference phase of ±90°. However, it was found that the quantization efficiencies of the two peaks were unbalanced for the asymmetric phase differences, i.e., $\Delta\varphi_{1\text{-bit}} \neq 180°$. In these cases, the level of one peak was higher than that of the other.

The largest quantization efficiency of 53.6% was found, especially at the −90° reference phase in Fig. 8(a), with the 140° phase difference between the on and off states, which shows a significant enhancement (=4.6%p or 9.3%) in efficiency compared to that of the conventional 180° phase difference [5], [6], [7].

TABLE 1. Comparison of RRAs with similar aperture size.

	[5]	[7]	[8]	Proposed RRA
Tunable component	PIN diode	PIN diode	Varactor diode	PIN diode
Frequency	12.5 GHz	11.5 GHz	10.1 GHz	9.85 GHz
Unit cell size	$0.5\lambda_0$	$0.365\lambda_0$	$0.45\lambda_0$	$0.34\lambda_0$
Number of elements	10 × 10	14 × 14	7 × 7	12 × 12
Aperture size	$5 \times 5\ \lambda_0^2$	$5.1 \times 5.1\ \lambda_0^2$	$3.15 \times 3.15\ \lambda_0^2$	$4.1 \times 4.1\ \lambda_0^2$
F/D (offset angle)	0.95 (25°)	0.96 (17.5°)	0.85 (25°)	0.36 (25°)
Peak gain (Aperture eff.)	17.5 dBi (17.9%)	19.2 dBi (25.7%)	15.01 dBi (25.42%)	17.14 dBi (28%)
Beam scanning range	-50° ~ +50° in *xoz* plane & not provided in *yoz* plane	-30° ~ +60° in *xoz* plane & -60° ~ +60° in *yoz* plane	-50° ~ +50° in *xoz* plane & 0° ~ +50° in *yoz* plane	-60° ~ +60° in both *xoz* and *yoz* plane
1dB bandwidth	~700 MHz (=5.1%)	~300 MHz (=2.61%)	~450 MHz (=4.4%)	530 MHz (=5.38%)

From the 25° feed offset angle of the proposed RRA and the result of the incident angle of 25° in Fig. 1(d), the frequency at which 180° phase difference appeared was 10.1 GHz, and the frequency at which 140° phase difference appeared was at 9.85 GHz. The calculated quantization efficiency for the 140° phase difference is plotted in the same domain with the simulated and measured aperture efficiencies at 9.85 GHz, as shown in Fig. 8(b). Furthermore, aperture efficiency is heavily correlated with quantization efficiency, and this correlation was also confirmed through the measured aperture efficiency. In conclusion, the phase difference between on and off states is not necessarily 180° for the maximum aperture efficiency.

Table 1 compares the performance of the proposed RRA with those of previously reported RRAs with similar aperture size. The reason for comparing previous RRAs with similar aperture size is that RRAs with a large aperture will have a wider beam scanning range due to the pencil beam-shaped array factor. The proposed RRA has the widest beam scanning range compared with [5], [7], [8]. It can be analyzed as a result of the wide element pattern due to the miniaturized unit cell. Despite the lowest F/D, the proposed RRA has the highest aperture efficiency. It is mainly due to the well-optimized aperture efficiency, such as asymmetric phase difference, reference phase, and feed position. In addition, 1dB gain bandwidth of the proposed RRA is similar/higher than previous RRAs.

V. CONCLUSION

A wide-angle beam steerable RRA was presented based on the miniaturized radiating element. By optimizing the type and location of the feed horn, a low profile configuration resulting in F/D = 0.36 was achieved. The highly directive beam in 3-D beam forming was experimentally verified. The maximum aperture efficiency occurred at the asymmetrical phase difference between the on/off states, i.e., not equal to 180°. The performances of the proposed 12 × 12 RRA were verified with the 28% aperture efficiency at 9.85 GHz, a 1 dB gain bandwidth of 530 MHz, and ±60° wide beam steering in both the *H*- (*xoz*) and *E*- (*yoz*) planes.

REFERENCES

[1] S. V. Hum and J. Perruisseau-Carrier, "Reconfigurable reflectarrays and array lenses for dynamic antenna beam control: A review," *IEEE Trans. Antennas Propag.*, vol. 62, no. 1, pp. 183–198, Jan. 2014.
[2] P. Nayeri, F. Yang, and A. Z. Elsherbeni, "Beam scanning reflectarray antennas: A technical overview and state of the art," *IEEE Antennas Propag. Mag.*, vol. 57, no. 4, pp. 32–47, Aug. 2015.
[3] J. Huang and J. A. Encinar, *Reflectarray Antennas*, 1st ed. Hoboken, NJ, USA: Wiley, 2008.
[4] B. Rana, I.-G. Lee, and I.-P. Hong, "Experimental characterization of 2×2 electronically reconfigurable 1 bit unit cells for a beamforming transmitarray at X band," *J. Electromagn. Eng. Sci.*, vol. 21, no. 2, pp. 153–160, Apr. 2021.
[5] H. Yang, F. Yang, S. Xu, Y. Mao, M. Li, X. Cao, and J. Gao, "A 1-bit 10×10 reconfigurable reflectarray antenna: Design, optimization, and experiment," *IEEE Trans. Antennas Propag.*, vol. 64, no. 6, pp. 2246–2254, Jun. 2016.
[6] H. Yang, F. Yang, X. Cao, S. Xu, J. Gao, X. Chen, M. Li, and T. Li, "A 1600-element dual-frequency electronically reconfigurable reflectarray at X/Ku-band," *IEEE Trans. Antennas Propag.*, vol. 65, no. 6, pp. 3024–3032, Jun. 2017.
[7] H. Zhang, X. Chen, Z. Wang, Y. Ge, and J. Pu, "A 1-bit electronically reconfigurable reflectarray antenna in X band," *IEEE Access*, vol. 7, pp. 66567–66575, 2019.
[8] M. E. Trampler, R. E. Lovato, and X. Gong, "Dual-resonance continuously beam-scanning X-band reflectarray antenna," *IEEE Trans. Antennas Propag.*, vol. 68, no. 8, pp. 6080–6087, Aug. 2020.
[9] X. Li, Y. Wan, J. Liu, D. Jiang, T. Bai, K. Zhu, J. Zhuang, and W.-Q. Wang, "Broadband electronically scanned reflectarray antenna with liquid crystals," *IEEE Antennas Wireless Propag. Lett.*, vol. 20, no. 3, pp. 396–400, Mar. 2021.
[10] O. Bayraktar, O. A. Civi, and T. Akin, "Beam switching reflectarray monolithically integrated with RF MEMS switches," *IEEE Trans. Antennas Propag.*, vol. 60, no. 2, pp. 854–862, Feb. 2012.
[11] H. Kamoda, T. Iwasaki, J. Tsumochi, T. Kuki, and O. Hashimoto, "60-GHz electronically reconfigurable large reflectarray using single-bit phase shifters," *IEEE Trans. Antennas Propag.*, vol. 59, no. 7, pp. 2524–2531, Jul. 2011.
[12] E. Carrasco, M. Barba, and J. A. Encinar, "X-band reflectarray antenna with switching-beam using PIN diodes and gathered elements," *IEEE Trans. Antennas Propag.*, vol. 60, no. 12, pp. 5700–5708, Dec. 2012.
[13] A. Yu, F. Yang, A. Z. Elsherbeni, J. Huang, and Y. Rahmat-Samii, "Aperture efficiency analysis of reflectarray antennas," *Microw. Opt. Technol. Lett.*, vol. 52, pp. 364–372, Sep. 2010.
[14] C. Lee, T. V. Hoang, S. W. Chi, S. Lee, and J. Lee, "Low profile quad-beam circularly polarised antenna using transmissive metasurface," *IET Microw., Antennas Propag.*, vol. 13, no. 10, pp. 1690–1698, Aug. 2019.
[15] C.-H. Lee and J.-H. Lee, "Wide angle scanning circular polarized meta-structured antenna array," *IEICE Trans. Commun.*, vol. 101, no. 9, pp. 2017–2023, Sep. 2018.
[16] C. A. Balanis, *Antenna Theory: Analysis and Design*, 4th ed. Hoboken, NJ, USA: Wiley, 2016.
[17] P. Hannan, "The element-gain paradox for a phased-array antenna," *IEEE Trans. Antennas Propag.*, vol. AP-12, no. 4, pp. 423–433, Jul. 1964.

SUN-GYU LEE received the B.S. and M.S. degrees in electronic and electrical engineering from Hongik University, Seoul, South Korea, in 2016 and 2018, respectively, where he is currently pursuing the Ph.D. degree. His research interests include metasurfaces antenna, retrodirective metasurface, metamaterial RF devices, and phased array antennas.

YONG-HYUN NAM received the B.S. and M.S. degrees from the Department of Electronic and Electrical Engineering, Hongik University, South Korea, in 2018 and 2020, respectively, where he is currently pursuing the Ph.D. degree with the Department of Electronic and Electrical Engineering. His research interests include metamaterial radio frequency devices and wireless power transfer.

YONGJUNE KIM (Member, IEEE) was born in Daejeon, South Korea, in 1984. He received the B.S. and Ph.D. degrees in electrical and electronic engineering from Yonsei University, South Korea, in 2008 and 2016, respectively. From 2016 to 2017, he was a Postdoctoral Researcher with the National University of Singapore. From 2017 to 2020, he worked with the Center for Advanced Meta-Materials as a Senior Researcher. From 2020 to 2022, he worked with the Metamaterial Electronic Device Research Center, Hongik University, as a Research Professor. He is currently an Assistant Professor with the Department of Electrical Engineering, The University of Suwon. His current research interests include electromagnetic metamaterial absorbers, cloaks, and metasurface antennas.

JONGYEONG KIM received the B.S. and M.S. degrees in electrical and electronics engineering from Chung-Ang University, South Korea, in 2018 and 2020, respectively.

Since 2021, he has been a Research Engineer with Hanwha Systems, South Korea. His current research interests include metasurface antenna and phased array antenna, RF systems, and RADAR systems.

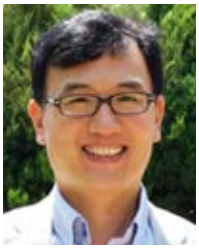

JEONG-HAE LEE (Senior Member, IEEE) received the B.S. and M.S. degrees in electrical engineering from Seoul National University, South Korea, in 1985 and 1988, respectively, and the Ph.D. degree in electrical engineering from the University of California at Los Angeles, in 1996. From 1993 to 1996, he was a Visiting Scientist with General Atomics, San Diego, CA, USA, where his major research initiatives were developing a millimeter-wave diagnostic system and studying plasma wave propagation. Since 1996, he has been working with the Department of Electronic and Electrical Engineering, Hongik University, Seoul, South Korea, as a Professor. He has more than 120 articles published in journals and 70 patents. He was the President of the Korea Institute of Electromagnetic Engineering and Science, in 2019. He is currently the Director of the Metamaterial Electronic Device Center. His current research interests include metamaterial radio frequency devices and wireless power transfer.